

Multitask Multimodal Fusion with Tabular Foundation Models for Peak and Durability Prediction of Pertussis Booster Response

Divya Sitani

Berlin, Germany

Abstract

Pertussis booster vaccination produces immune responses that vary widely across individuals in both peak magnitude and long-term durability. These two phases are governed by partly distinct biological compartments: peak reflects acute B-cell activation and antibody secretion, while durability reflects the establishment of long-term humoral memory [1, 2]. Yet most computational models target only one, missing the full boost-and-wane trajectory. Jointly predicting both is non-trivial because the two endpoints are biologically dissociated rather than redundant; samples are small, modalities are heterogeneous with structured missingness, and the two tasks rely on different measurement windows.

We propose a multi-task contrastive multimodal fusion architecture combining frozen TabPFN-v2 per-modality encoders, a dual-label supervised contrastive loss that treats two subjects as a positive pair if they agree on the Task 1 label or the Task 2 label, modality dropout calibrated to empirical missingness, and missingness-masked attention fusion. Applied to the curated subset of CMI-PB data [3] ($n = 158$ subjects, four modalities, 44.9% with at least one modality missing; Spearman $r = -0.58$ between peak and durability, $n = 96$), the model achieves test area under the receiver operating characteristic curve (AUROC) 0.797 (95% confidence interval [CI] [0.621, 0.948]) for peak response and 0.755 (95% CI [0.519, 0.945]) for durability, with both significant under joint label permutation ($N = 1000$; $p = 0.002$ and $p = 0.045$). Across logistic regression, XGBoost, and MLP baselines on raw features and on TabPFN embeddings, the proposed model is the only one whose 95% CIs lie above chance on both tasks simultaneously. Per-modality contribution analyses recover task-specific modality contributions consistent with the underlying immunology: peak prediction is carried by cytokine signatures, while durability is carried by baseline antibody features.

Introduction

Pertussis, or whooping cough, has re-emerged as a significant public health concern despite high vaccination coverage in many countries [4, 5]. The introduction of acellular pertussis (aP) vaccines in the 1990s, motivated by the reactogenicity of earlier whole-cell pertussis (wP) formulations, reduced adverse events but introduced a new challenge: aP-induced immunity wanes more rapidly than wP-induced immunity, and aP vaccination fails to prevent colonization and transmission of *Bordetella pertussis* [6]. Epidemiological studies have documented disproportionately high pertussis rates among adolescents and young adults who received exclusively aP vaccines in childhood [7], and immunological investigations have revealed qualitative differences in the immune memory established by the two vaccine types. Whole-cell vaccines induce a Th1/Th17-polarized response and respiratory tissue-resident memory T cells that can persist for decades [8, 9], consistent with murine studies showing wP-induced T_{RM} -mediated mucosal protection [10], whereas acellular vaccines elicit a Th2-biased, antibody-focused response that is effective against disease but less durable and less capable of preventing nasal colonization in animal models [6, 11]. Understanding what determines the strength and longevity of booster responses, and how these differ between priming regimens, is central to improving pertussis vaccination strategies.

A critical but underappreciated aspect of vaccine response assessment is that response magnitude and response durability are not the same quantity measured at two timepoints; they are biologically distinct processes with partially opposing dynamics. Subjects who mount the strongest peak antibody responses after boosting often exhibit the most rapid subsequent decline: the “boost-and-wane” trade-off, reflecting partly distinct biological programs governing acute and long-term humoral responses [1, 2]. This dissociation has practical consequences: a subject classified as a strong responder at day 14 may be a poor retainer at day 120, and vice versa. Yet most computational models of vaccine response treat prediction as a single-task problem, typically targeting peak antibody titer or fold change alone. This conflation obscures the distinct immunological programs underlying each phase and misses the clinically relevant question of whether a given individual will sustain protective antibody levels over months to years. Jointly modeling both response phases, while respecting their biological independence, requires a multi-task learning framework that can leverage shared structure without forcing the two outcomes onto a single predictive axis.

The CMI-PB (Computational Models of Immunity: Pertussis Boost) project [3] provides a uniquely suited resource for this challenge, building on the systems vaccinology paradigm pioneered by predictive analyses of yellow fever and influenza responses [12]. CMI-PB has profiled pertussis booster vaccine responses across four annual cohorts (2020-2023) using four data modalities: antibody titers, cytokine concentrations, cell frequencies, and gene expression. The dataset has been the basis for community prediction challenges, in which participants attempt to predict immune response outcomes from pre-vaccination measurements [3]. However, prior modeling efforts have largely been single-task (predicting peak antibody response only), single-modality (using one data type at a time or simple concatenation), and have not addressed the substantial structured missingness inherent in multi-omic clinical data, where 44.9% of subjects in the Task 1 subset lack one or more complete modalities, with missingness rates that can be up to 38.6% (cytokine).

Tabular foundation models such as TabPFN [13] have recently demonstrated strong performance on small tabular classification problems through in-context learning, but their application to multimodal health data with heterogeneous missingness remains largely unexplored. The combination of small sample size ($n = 158$ subjects with the primary label, $n = 96$ of these additionally with the durability label), four heterogeneous modalities, structured missingness, and two biologically anti-correlated prediction tasks makes pertussis booster response prediction a compelling testbed for multimodal learning methods designed for the small-data regime.

Here, we propose a multi-task contrastive multimodal fusion architecture for jointly predicting peak and durability of pertussis booster antibody response. The model encodes each data modality independently using frozen TabPFN-v2 embeddings [14], projects them to a shared representation space via independent projection heads with l_2 normalization, and aligns cross-modal embeddings using a dual-label supervised contrastive loss that treats subjects as positive pairs if they share the same label on either task. Modality dropout during training, calibrated to the empirical missingness rate, ensures robustness to arbitrary patterns of missing modalities at inference time. Attention-weighted fusion with missingness-aware renormalization combines available modality representations, which then pass through a shared MLP before

branching into task-specific classification heads.

Applied to CMI-PB data, the model achieves test AUROC 0.797 for peak response and 0.755 for durability, with bootstrap 95% confidence intervals quantifying uncertainty on both estimates, and joint label-permutation tests ($N = 1000$) rejecting the null of no feature-label relationship at $p = 0.002$ (Task 1) and $p = 0.045$ (Task 2). Beyond predictive performance, per-modality contribution analyses reveal that different modalities matter for different tasks (Fig 7): for peak prediction, cytokine signatures both dominate as the standalone predictor and are the only modality whose removal materially harms the ensemble; for durability, antibody features carry most of the information. We further observe an asymmetric peak-durability dissociation (Fig 3): the “low-peak/low-durability” quadrant is essentially empty, with subjects instead sorting into a “big-and-fading” or “modest-and-durable” response strategy. Architectural ablations (Table 3) show that both the dual-label contrastive loss and modality dropout contribute substantial, non-redundant performance gains, with a non-trivial interaction between them.

Materials and methods

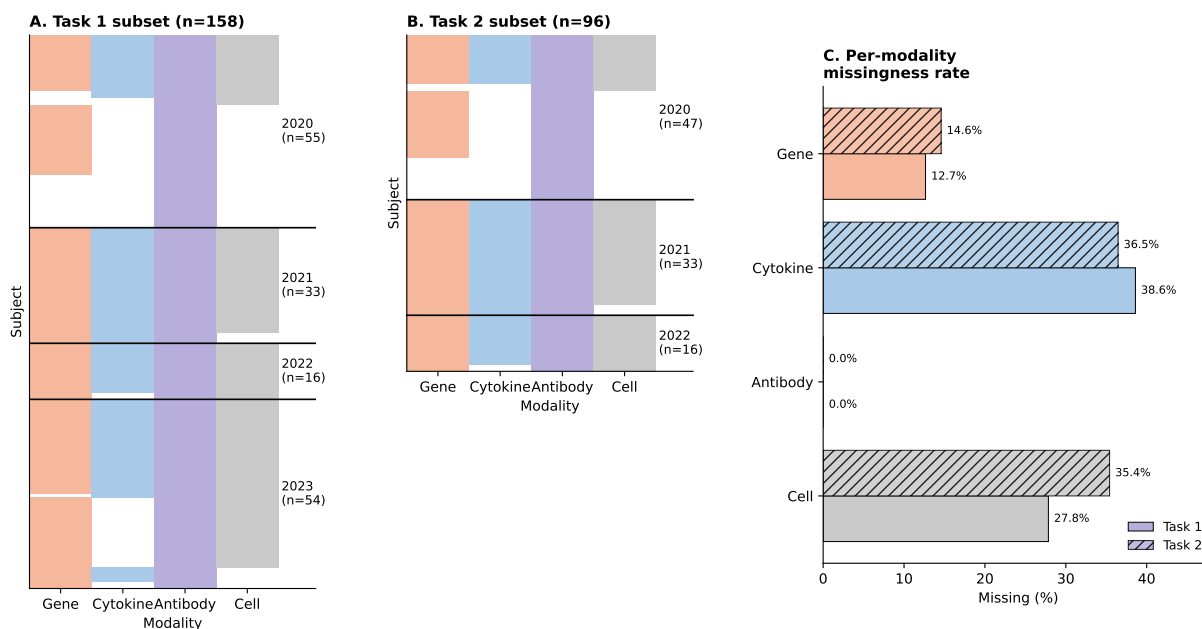
Dataset

We use the CMI-PB (Computational Models of Immunity: Pertussis Boost) dataset [3], a longitudinal multi-omic resource designed for benchmarking computational models of pertussis booster vaccination response. The dataset comprises immune profiling of subjects receiving a pertussis booster vaccination (Tdap), and we use four data modalities from CMI-PB measured across multiple timepoints: plasma antibody titers (IgG subtype responses to pertussis and control antigens), plasma cytokine concentrations (Olink NPX), peripheral blood mononuclear cell (PBMC) frequencies by flow cytometry, and PBMC gene expression (bulk RNA-seq). All four modalities were batch corrected by the CMI-PB consortium using the standardized pipeline described at <https://github.com/CMI-PB/cmi-pb-3rd-public-challenge-data-prep>: KNN imputation of missing values [15], median normalization per dataset, and ComBat based batch correction [16] of annual cohort-level batch effects [3]. Subjects span four annual cohorts (2020–2023). From the CMI-PB resource, we retained subjects with at least one of the four modalities measured and an available label, yielding $n = 158$ for Task 1 (peak) and $n = 102$ for Task 2 (durability), with $n = 96$ subjects in common. The 2023 cohort lacks day 120 antibody measurements and is therefore automatically excluded from Task 2 via masking of missing labels. The modeled dataset now consists of the $n = 158$ subjects with a Task 1 label and at least one modality; $n = 4$ subjects with a Task 2 label but no Task 1 label are excluded so that every modeled subject contributes to the primary task. Of the 158 modeled subjects, $n = 96$ additionally carry a Task 2 label and contribute to the durability head via masked loss (Fig. 1; see the *Data split* section below).

Modality availability varies by cohort and assay. In the Task 1 subset ($n = 158$): antibody titers are nearly complete (0% missing), gene expression is also quite complete (12.7% missing), while cell frequency (27.8%) and cytokine (38.6%) show substantial missingness. Only 55.1% of Task 1 subjects have all four modalities; 44.9% are missing at least one (Fig 1). The Task 2 modeling subset ($n = 96$) shows a similar overall pattern, with cell, cytokine, and gene missingness rates of 35.4%, 36.5%, and 14.6% respectively; 39.6% of Task 2 subjects are missing at least one modality. This missingness is structured rather than random: it is driven primarily by assay availability at the cohort level (certain modalities were not collected in certain cohort years) rather than by subject-level dropout. This motivates an architecture that handles arbitrary modality subsets at both training and inference time, since restricting to complete-data subjects would exclude entire cohorts.

Prediction tasks

We define two complementary binary classification tasks reflecting biologically dissociated phases of the humoral response to pertussis booster vaccination.



Task 1: 71/158 subjects (44.9%) missing ≥ 1 modality | Task 2: 38/96 subjects (39.6%) missing ≥ 1 modality

Fig 1. Cohort \times modality missingness pattern in CMI-PB. (A) Subject level modality availability for the Task 1 (peak response) cohort, organised by annual cohort (2020-2023). Each row is one subject; each column is one of the four data modalities. Filled cells indicate the modality is present; white cells indicate it is missing. Within each cohort, subjects are sorted by missingness pattern (subjects with more modalities at the top). Horizontal black lines separate cohorts. (B) The same visualization restricted to the Task 2 (durability) modelling subset: subjects with both a Task 1 and a Task 2 label ($n = 96$). Subjects with a Task 2 label but no Task 1 label ($n = 4$) are not modeled and are excluded here. The 2023 cohort is absent because antibody measurements at day 120 were not collected for that year. (C) Per-modality missingness rate within each task subset. The pattern reveals that missingness is structural and cohort driven, rather than reflecting random subject dropout: certain modalities were systematically not collected in certain cohort years. This motivates an architecture that handles arbitrary modality subsets at both training and inference time.

Task 1 (primary): peak response.

The primary prediction target is the \log_2 fold change of IgG anti-pertussis toxin (IgG-PT) antibody titer from day 0 to day 14:

$$\text{FC}_{\text{peak}} = \log_2 \left(\frac{\text{IgG-PT}_{d14} + 1}{\text{IgG-PT}_{d0} + 1} \right) \quad (1)$$

A binary responder label is derived by median split (cutoff 1.254). By childhood vaccination history, wP-primed subjects are disproportionately responders (47 responder / 32 non-responder), while aP-primed subjects are disproportionately non-responders (31 / 48), consistent with the established wP advantage in peak response magnitude. Pertussis toxin (PT) is the only antigen unique to *Bordetella pertussis*; anti-PT IgG is the standard serological correlate of pertussis-specific immunity and the primary endpoint in CMI-PB challenges [3].

Task 2 (secondary): durability / retention

The secondary prediction target captures antibody retention between the near-peak timepoint (day 30) and long-term follow-up (day 120):

$$\text{FC}_{\text{retention}} = \log_2 \left(\frac{\text{IgG-PT}_{d120} + 1}{\text{IgG-PT}_{d30} + 1} \right) \quad (2)$$

The denominator uses d30 rather than d0 to avoid a ceiling effect artifact in the shared baseline that would otherwise produce a spurious positive correlation between peak and retention. The binary durability label is derived by median split. A total of $n = 102$ subjects have complete d30 and d120 measurements (2020-2022 cohorts); of these, $n = 96$ also carry a Task 1 label and constitute the modeled Task 2 cohort. The remaining $n = 4$ subjects with Task 2 labels but no Task 1 label are excluded. Median \log_2 retention is -0.464 , corresponding to a typical $\sim 28\%$ loss of d30 antibody level by d120. Missing Task 2 labels in the modeling subset ($n = 62$ subjects without a d120 measurement, primarily the 2023 cohort) are encoded as -1 and handled by masked loss during training.

Peak-durability dissociation

The two tasks capture anti-correlated biology: Spearman $r = -0.580$ ($p = 3.97 \times 10^{-10}$, $n = 96$); Cohen’s $\kappa = -0.520$ on the binary labels (Fig 3). A strong peak responder is substantially more likely to exhibit poor retention: the so-called “boost-and-wane” pattern [2]. The two tasks are therefore statistically dissociated rather than redundant, motivating the multi-task design.

Input feature design

Input features consist of baseline day 0 values and \log_2 fold changes at non-label timepoints (Table 1). Day 1 features are included for cytokine and cell frequency, which capture fast innate-response dynamics that peak within 24-48 hours of booster administration [12, 17]. Antibody and gene expression skip day 1: antibody titers do not change appreciably one day after a booster, and the most informative transcriptional signatures of vaccine response have been shown to emerge at day 7 [18, 19].

For linear-scale modalities (antibody, cell): $\text{lfc}(f, t) = \log_2((f_t + 1)/(f_0 + 1))$. For log-scale modalities (cytokine NPX, gene expression): $\text{lfc}(f, t) = f_t - f_0$.

Two metadata features, childhood vaccine type (wP/aP) and biological sex, are concatenated after fusion (see *Model architecture* below). Subjects lacking specimens at any of the timepoints required by the four modalities (Table 1) were excluded from analysis. After this filter, $n = 158$ for Task 1 and $n = 96$ for Task 2.

Label-feature separation

Because both tasks are derived from IgG-PT measurements at different timepoints, care is needed to ensure that no feature used as input also appears in label construction. We apply three checks during feature generation.

Table 1. Per-modality experimental design. Label-defining timepoints excluded from inputs. The PT family (IgG-PT and its four subclasses IgG1-PT, IgG2-PT, IgG3-PT, IgG4-PT) are removed from antibody inputs at all timepoints (d0, d3, d7, d30) to avoid proximal label leakage. Δ_t : \log_2 fold change from baseline at day t .

Modality	Input features	Timepoints	d1 used?
Antibody	$x_0, \Delta_3, \Delta_7, \Delta_{30}$; PT family removed at all timepoints	d0, d3, d7, d30	No
Cytokine	$x_0, \Delta_1, \Delta_7, \Delta_{14}$	d0, d1, d7, d14	Yes
Cell freq	$x_0, \Delta_1, \Delta_3, \Delta_{14}$	d0, d1, d3, d14	Yes
Gene expr	$x_0, \Delta_7, \Delta_{14}$	d0, d7, d14	No

First, day 14 antibody measurements are excluded from the input features entirely, since they form the Task 1 numerator (\log_2 d14/d0 IgG-PT). Day 120 measurements are never used as inputs either; they form the Task 2 numerator (\log_2 d120/d30 IgG-PT).

Second, pertussis-toxin-specific antibody features (IgG-PT and its four subclasses IgG1-PT, IgG2-PT, IgG3-PT, IgG4-PT) are removed from the antibody input table *at every input timepoint* (day 0, day 3, day 7, day 30). Although days 3 and 7 do not directly enter either label, retaining them risks proximal label leakage because anti-PT IgG titers are autocorrelated within a subject across days; we therefore exclude the entire PT family from the antibody inputs. Anti-PT signal is still represented in the model via the d3 and d7 IgG titers of *other* pertussis antigens (FIM2/3, FHA, PRN), which are also components of the acellular vaccine and which elicit correlated antibody responses upon boosting [20, 21], but are not direct label constituents.

Third, gene expression preprocessing (variance filtering to the top 2,000 features and standardization) is fit on training data only, then applied to validation and test data without re-fitting. This prevents test set statistics from influencing feature selection or scaling.

Model architecture

The architecture (Fig 2) is a discriminative multi-task contrastive multimodal fusion model. It takes per-subject feature tables from four immune modalities, produces a single fused 64-dimensional representation, and predicts two binary classification targets jointly. Three design choices address the core challenges at this sample size: frozen pretrained TabPFN-v2 encoders make each modality individually informative without requiring per-modality training on our small dataset; modality dropout and missingness-masked attention fusion let the model train and infer under arbitrary subsets of missing modalities; and a dual-label supervised contrastive loss transfers information across subjects by comparing pairs, despite having only a few dozen subjects per class.

Inputs

For each modality, the input is a feature table with subject-specific baseline values and log-fold-change columns at pre-label timepoints: antibody (day 0, 3, 7, 30; day 14 excluded as the Task 1 label timepoint, and the PT family (IgG-PT and its four subclasses IgG1-PT, IgG2-PT, IgG3-PT, IgG4-PT) removed at all input timepoints to avoid proximal label leakage), cytokine (day 0, 1, 7, 14), cell frequency (day 0, 1, 3, 14), and gene expression (day 0, 7, 14). Gene expression is pre-filtered by variance to the top 2,000 features on the training set before encoding. Metadata (`infancy_vac`, biological sex) is held aside as a two-dimensional auxiliary input.

Modality availability varies across subjects. Antibody is nearly fully observed (0% missing); gene expression is also nearly complete (12.7% missing); cell frequency and cytokine are more sporadic (27.8% and 38.6% missing respectively, in the Task 1 subset). In aggregate, 44.9% of subjects lack at least one complete modality. Missingness is at the level of entire modalities, not individual features, and is driven primarily by cohort-level assay availability rather than random dropout.

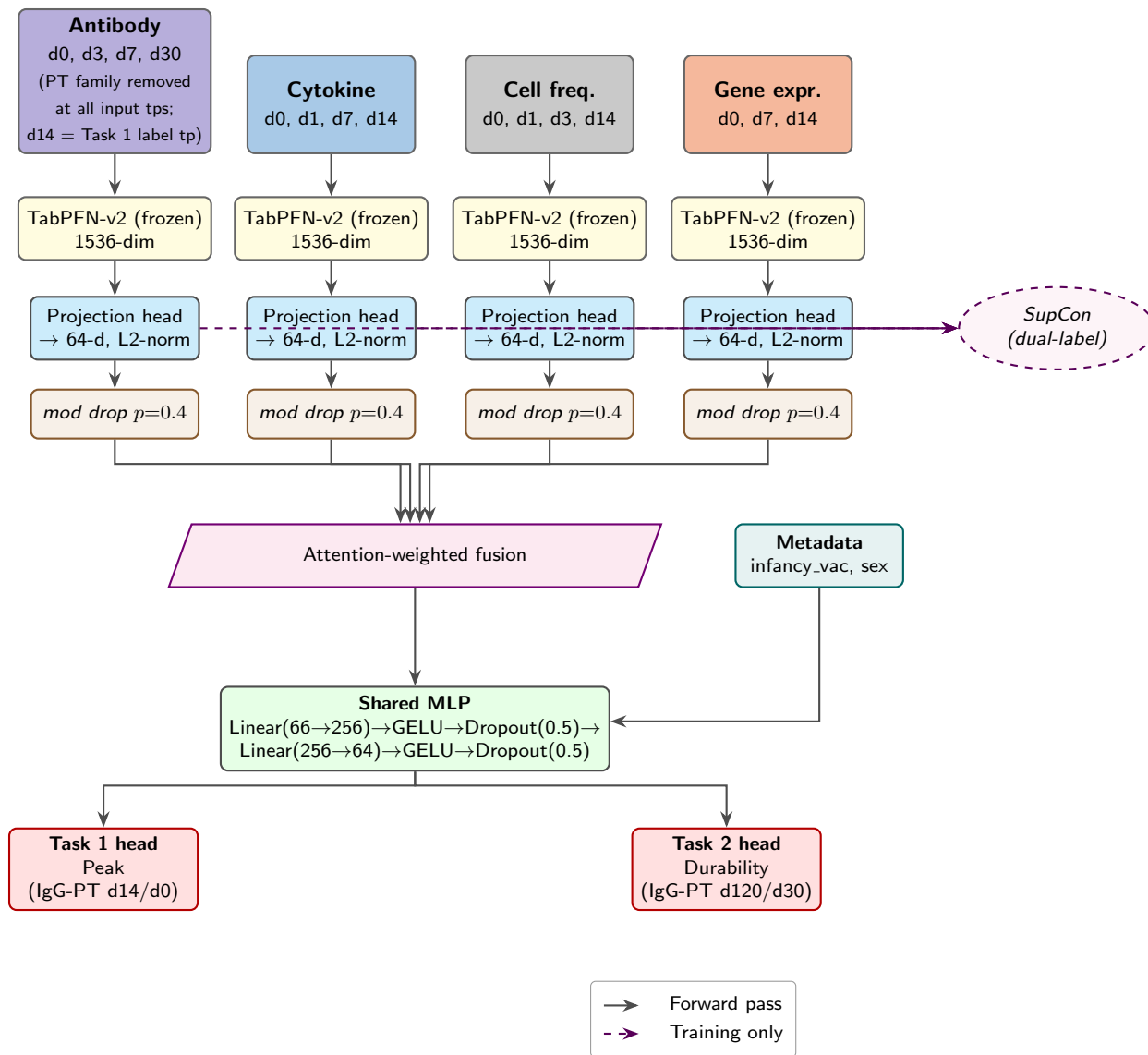


Fig 2. Multi-task contrastive multimodal fusion architecture. Four immune modalities are independently encoded by frozen TabPFN-v2 encoders and projected to a shared 64-dim space via per-modality MLP heads with l_2 normalization. A dual-label supervised contrastive loss (dashed arrows; training only) aligns same-class representations across modalities. Modality dropout ($p = 0.4$; training only) masks each modality independently to encourage robustness to missing inputs. An attention-weighted fusion layer combines present modalities into a single representation, which is concatenated with subject metadata (infancy_vac, biological sex), passed through a shared MLP, and branched into two classification heads: Task 1 (peak response, \log_2 IgG-PT day 14/day 0) and Task 2 (durability, \log_2 IgG-PT day 120/day 30).

Per-modality TabPFN-v2 encoders (frozen)

Each modality’s feature table is passed through a frozen TabPFN-v2 [13,14] tabular foundation model, which returns a 1,536-dimensional in-context embedding per subject. TabPFN-v2 is pre-trained on a large corpus of synthetic tabular tasks and produces meaningful embeddings for new tables without fine-tuning. We use it as a frozen feature extractor: the encoder weights do not change during training. At our sample size (a few dozen subjects per modality after splitting), training a separate encoder per modality from scratch would overfit; TabPFN-v2 imports pretrained structure we could not afford to learn ourselves.

Projection heads

Independent two-layer MLP projection heads $g_m(\cdot)$, one per modality, map each modality’s 1,536-dimensional TabPFN embedding into a shared 64-dimensional space (hidden dimension 256), followed by ℓ_2 -normalization:

$$\mathbf{h}_m^{(i)} = \frac{g_m(\mathbf{z}_m^{(i)})}{\|g_m(\mathbf{z}_m^{(i)})\|_2}, \quad g_m(\mathbf{z}) = W_2^{(m)} \sigma\left(\text{LN}(W_1^{(m)} \mathbf{z} + \mathbf{b}_1^{(m)})\right) + \mathbf{b}_2^{(m)} \quad (3)$$

where σ is GELU activation and LN is layer normalization (dropout between activation and the second linear layer is omitted for clarity; see Table 2). There is no weight sharing across modalities: antibody, cytokine, cell frequency, and gene expression carry fundamentally different biological information, and a per-modality projection preserves modality-specific structure that a shared head would average over. The ℓ_2 normalization places the projected embeddings on the unit sphere, which is the geometric setting required by the supervised contrastive loss below [22].

Dual-label supervised contrastive loss

A supervised contrastive (SupCon) loss [22] operates on the normalized projections $\mathbf{h}_m^{(i)}$ during training only (dashed arrows in Fig 2). The loss pulls together the embeddings of subjects designated as a *positive pair* and pushes apart those of *negative pairs*. We extend single-label SupCon to a *dual-label* variant: two subjects form a positive pair if they agree on the Task 1 label *or* the Task 2 label, so both tasks have equal influence on the learned geometry. When the Task 2 label is missing (2023 cohort, encoded as -1), subjects participate in positive-pair construction via their Task 1 label alone. Temperature $\tau = 0.3$; contrastive weight $\lambda = 0.1$. We use the “OR” definition instead of “AND” because Task 1 and Task 2 labels are strongly anti-correlated (Spearman $r = -0.58$), so requiring agreement on both would produce too few positive pairs per batch to train a stable contrastive objective.

Modality dropout

During training, each of the four modalities is independently zeroed with probability $p = 0.4$ on each forward pass, with the constraint that at least one modality is always retained. Dropout is applied per subject per step, so the same subject is seen through different modality subsets across different training steps. Over an epoch, the model is exposed to a wide range of modality combinations. The per-modality rate $p = 0.4$ is set in the same range as the empirical per-modality missingness rates in the Task 1 subset, which lie between 0% (antibody) and 38.6% (cytokine). Note that under independent per-modality dropout at $p = 0.4$, the probability that at least one modality is dropped on a given forward pass is $1 - (1 - p)^4 = 1 - 0.6^4 = 0.87$ (slightly lower in practice because the all-dropped case ($p^4 = 0.026$) is prevented). This exceeds the 44.9% rate at which subjects in the Task 1 subset are missing at least one modality. The training time dropout regime is therefore deliberately more aggressive than the inference time missingness pattern, in order to encourage robustness to modality combinations that may not be represented in the training set. The purpose is to ensure that any modality combination encountered at inference, including subjects missing any subset of the four modalities, is in-distribution for the trained model rather than a distribution shift. Modality dropout is switched off at inference; practical missingness at test time is handled by the attention fusion below.

Attention-weighted fusion with missingness masking

A learned query vector $\mathbf{w} \in \mathbb{R}^{64}$ computes attention scores over the present modalities for each subject. Critically, modalities that are absent (whether due to real missingness or modality dropout during training) are excluded from the softmax computation, so that the attention weights are computed and normalized only over the subset of modalities that are actually observed:

$$\alpha_m^{(i)} = \frac{\exp(\mathbf{w}^\top \mathbf{h}_m^{(i)})}{\sum_{m': \mu_{m'}^{(i)}=1} \exp(\mathbf{w}^\top \mathbf{h}_{m'}^{(i)})} \quad \text{for } m \text{ with } \mu_m^{(i)} = 1, \quad \mathbf{f}^{(i)} = \sum_{m=1}^M \mu_m^{(i)} \cdot \alpha_m^{(i)} \cdot \mathbf{h}_m^{(i)} \quad (4)$$

where $\mu_m^{(i)} \in \{0, 1\}$ indicates whether modality m is present for subject i . The weights $\alpha_m^{(i)}$ sum to one over the observed modalities, so the fused representation is a convex combination of the available modalities with no imputation or placeholder values. The same fusion code handles training (with dropout-induced missingness) and inference (with real missingness) without any mode switch.

Metadata injection into the shared MLP

The 64-dimensional fused representation $\mathbf{f}^{(i)}$ is concatenated with a 2-dimensional binary metadata vector (childhood priming and biological sex), yielding a 66-dimensional input to the shared MLP: Linear(66 \rightarrow 256) \rightarrow GELU \rightarrow Dropout(0.5) \rightarrow Linear(256 \rightarrow 64). Metadata is injected after fusion rather than as a fifth fusion modality. This choice has an important interpretability consequence: because the attention layer never sees `infancy_vac`, it cannot learn to route modality attention based on priming status.

Task heads

Two linear classification heads branch from the shared MLP output, each producing 2-class logits: Task 1 (peak response) and Task 2 (durability). Each head is a single Linear(64 \rightarrow 2) with no head-specific hidden layers. Keeping the heads linear forces task-discriminative structure to live in the shared MLP, where it is constrained to also serve the other task. A non-linear per-task head would let each task silently build a specialized representation that diverges from the shared one, which would defeat the purpose of multi-task learning.

Joint training objective

Total loss is

$$\mathcal{L} = \mathcal{L}_{\text{CE}}^{(\text{T1})} + w_{\text{T2}} \cdot \mathcal{L}_{\text{CE}}^{(\text{T2})} \cdot \mathbf{1}[y_{\text{T2}} \neq -1] + \lambda \cdot \mathcal{L}_{\text{con}} \quad (5)$$

with $w_{\text{T2}} = 2.0$ and $\lambda = 0.1$. The Task 2 cross-entropy is masked for subjects without day-120 measurements (2023 cohort) but those subjects still contribute to Task 1 cross-entropy and to the dual-label SupCon loss via their Task 1 label. Optimization uses AdamW [23]: learning rate 10^{-2} , weight decay 10^{-3} , cosine annealing schedule, gradient clipping at norm 1.0, batch size 32, up to 60 epochs, early stopping on mean validation AUROC with patience 10. The Task 2 loss is up-weighted ($w_{\text{T2}} = 2$) to compensate for the missing-label masking that excludes the 2023 cohort from the Task 2 cross-entropy term, which would otherwise underrepresent the durability gradient signal during training. The choice is validated empirically against $w_{\text{T2}} = 1$ in Table 3.

Full hyperparameter configuration in Table 2.

Data split

We use a fixed stratified train/validation/test split (fixed seed) yielding $n_{\text{train}} = 94$, $n_{\text{val}} = 32$, and $n_{\text{test}} = 32$ subjects for Task 1. For Task 2 (durability), the test set contains $n = 21$ subjects with non-missing retention labels. We use the hyperparameters in Table 2 throughout. Earlier exploratory Optuna searches across multiple seeds and hyperparameter ranges did not produce a configuration that consistently outperformed hand-chosen defaults on validation, likely because the validation set ($n = 32$) is too small to reliably distinguish small performance differences between configurations. We therefore did not re-run a full hyperparameter search on the final feature design and report results at the default configuration shown.

Table 2. Hyperparameter configuration.

Hyperparameter	Value
Projection dim / hidden	64 / 256
Shared MLP hidden dims	(256, 64)
Dropout	0.5
Contrastive weight (λ) / temperature (τ)	0.1 / 0.3
Modality dropout (p)	0.4
Task 2 weight (w_{T2})	2.0
Learning rate / weight decay	10^{-2} / 10^{-3}
Batch size / max epochs / patience	32 / 60 / 10

Experimental design

Permutation test

To assess whether predictive performance is distinguishable from chance, we perform a label-shuffling permutation test [24] applied jointly to both tasks. For each of $N = 1000$ permutations, we (i) randomly shuffle the Task 1 labels across all subjects in the full cohort, (ii) independently shuffle the Task 2 labels across subjects that have them (preserving the Task 2 missingness pattern), (iii) retrain the full pipeline from scratch on the shuffled dataset using the same fixed seed train/validation/test split and the same hyperparameters, and (iv) record the resulting test-set AUROC for both tasks. These N AUROCs form the null distribution: the performance the architecture would achieve if the feature-label relationship were random. The one-sided p -value for each task is

$$p = \frac{1 + \sum_{i=1}^N \mathbf{1}[\text{null}_i \geq \text{obs}]}{N + 1} \tag{6}$$

where obs is the observed test AUROC on the real, unshuffled labels.

Retraining from scratch on each permuted dataset ensures that the observed AUROC reflects a genuine, learnable feature-label relationship rather than a quirk of the split, hyperparameter choice, or initialization. Joint shuffling of both task labels preserves the validity of the null under the dual-label supervised contrastive loss, which otherwise would leak information from the unshuffled task during training.

Bootstrap confidence intervals

To quantify uncertainty on the observed test AUROCs, we compute bootstrap confidence intervals by resampling the test set with replacement. For each of $B = 1000$ resamples, we sample n_{test} subject indices uniformly with replacement from the held-out test set, compute AUROC on the resampled subjects using the trained model’s fixed predictions (without retraining), and record the value. Resamples in which the bootstrap sample contains only a single class (degenerate AUROC) are discarded. The 95% confidence interval is then the 2.5th and 97.5th percentiles of the resulting bootstrap distribution (percentile method). The architecture is evaluated on a single seed train/val/test split. Although the bootstrap confidence intervals quantify evaluation uncertainty given this split, they do not capture variability due to split selection or training stochasticity; multi-seed evaluation is deferred to subsequent work.

Per-modality contribution analyses

We use two complementary analyses to quantify what each modality contributes. *Leave-one-out (LOO)*: we recompute test AUROC with one modality masked out at inference (its mask set to zero, attention renormalized over the remaining three), repeated for each modality. *Keep-one-out (KOO)*: we recompute test AUROC keeping only one modality at inference, with the other three masked out. Both are conducted on the trained preferred model without retraining; the model itself is unchanged. LOO measures *additive contribution* (how much worse without modality m); KOO measures *standalone sufficiency* (how well modality m alone supports prediction). Together they diagnose whether a modality is necessary, sufficient, both, or neither.

Graceful degradation

To probe robustness to modality loss at deployment, we simulate a range of missingness severities at inference: for each modality, we randomly mask its values for a fraction $\rho \in \{0.0, 0.1, 0.2, 0.3, 0.5, 0.7, 1.0\}$ of test subjects and recompute test AUROC. The masking pattern is drawn under a fixed seed. A graceful degradation profile shows how AUROC varies with ρ , indicating how the missingness-aware fusion handles practical deployment where any subset of subjects might lack any subset of modalities.

Architectural ablation

We evaluate five configurations on the same train/val/test split as the main results: (i) *Full (preferred)* with contrastive loss ($\lambda = 0.1$), modality dropout ($p = 0.4$), and Task 2 upweighting ($w_{T2} = 2$); (ii) *No contrastive* ($\lambda = 0$) which removes the dual-label SupCon alignment; (iii) *No modality dropout* ($p = 0$) which disables the training-time random masking of modalities, so each subject is seen during training only with the modality combination they were measured under; (iv) *Neither*, with both contrastive and modality dropout removed; and (v) *No T2 up-weighting* ($w_{T2} = 1$) which removes the durability-loss compensation. The same seed is used throughout and the same hyperparameters otherwise. We report test AUROC and bootstrap 95% CI for both tasks.

Baseline comparisons

For benchmarking the multi-task fusion architecture, we trained three baseline classifiers on the concatenation of raw features from all four modalities (antibody, cytokine, cell frequency, gene expression): logistic regression from scikit-learn [25], gradient-boosted trees from XGBoost [26], and a small multilayer perceptron (*TabMLP*: two hidden layers of size 128 and 64 with GELU activation and dropout 0.3, trained with AdamW, cross-entropy loss, batch size 32, learning rate 10^{-3} , weight decay 10^{-4} , for 150 epochs). Missing modality values were imputed using per-feature training-set means; logistic regression and TabMLP additionally used training-set z-score standardisation, while XGBoost was trained on imputed-but-unstandardised features per its standard usage. All three baselines used the same seed as the rest of the code with the same train/test split as well, and the default hyperparameters (XGBoost: 100 trees, max depth 3, learning rate 0.1, histogram tree method; logistic regression: L_2 penalty, $C = 1.0$, LBFGS solver, max 2000 iterations). Task 2 baselines were fit only on subjects with a non-missing durability label. Test-set AUROC confidence intervals were computed by the same 1000-resample bootstrap used for the main results.

To isolate the contribution of the multi-task contrastive fusion architecture from the contribution of the underlying TabPFN-v2 feature extractor, we additionally evaluated the three baseline classifiers on concatenated TabPFN-v2 embeddings. For each subject, we generated a 1,536-dimensional TabPFN embedding per modality (using the same per-modality feature design as the main model) and concatenated them into a single 6,144-dimensional input vector, with subjects missing a modality assigned a zero vector for that modality’s embedding block. Logistic regression, XGBoost, and TabMLP were then trained on these concatenated embeddings using the same hyperparameters and train/test split as the raw-feature baselines.

Results

Peak and durability are anti-correlated

Peak fold change and durability retention are strongly negatively correlated (Spearman $r = -0.580$, $p = 3.97 \times 10^{-10}$, $n = 96$; Cohen’s $\kappa = -0.520$ on the binary labels; Fig 3). The 2×2 quadrant counts confirm the asymmetry: 44 subjects fall in high peak / low durability, 30 in low peak / high durability, 20 in high peak / high durability, and only 4 in low peak / low durability. The two tasks are statistically dissociated rather than redundant.

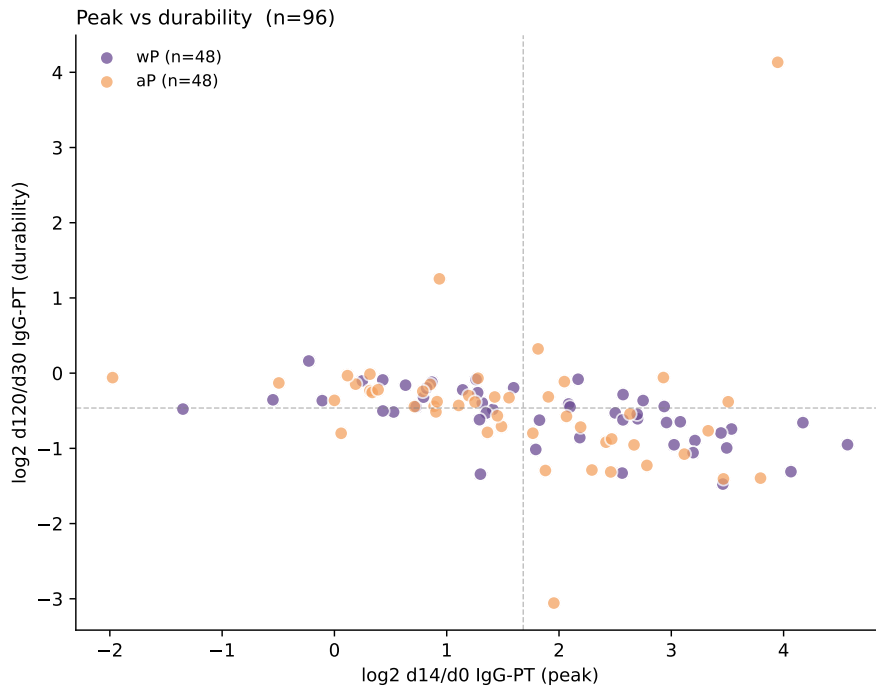


Fig 3. Peak and durability are anti-correlated phases of the humoral response. Scatter of \log_2 day 120/day 30 retention (durability, y-axis) versus \log_2 day 14/day 0 IgG-PT fold change (peak, x-axis) for the subjects with both labels available ($n = 96$). Subjects colored by childhood vaccination history. Dotted vertical line: peak median used to derive the Task 1 binary label. Dashed horizontal line: durability median used to derive the Task 2 binary label. The strong negative correlation (Spearman $r = -0.58$, $p = 4.0 \times 10^{-10}$; Cohen's $\kappa = -0.52$) reflects the dissociation between acute and long-term phases of the humoral response, motivating the multi-task framing. Childhood priming is significantly associated with the Task 1 binary label ($2 \times 2 \chi^2$ on priming \times peak: $p = 0.017$, OR ≈ 2.27) but does not by itself separate responders from non-responders, motivating the use of multimodal immune measurements on top of priming history as model inputs.

Test-set ROC with 95% bootstrap CI band

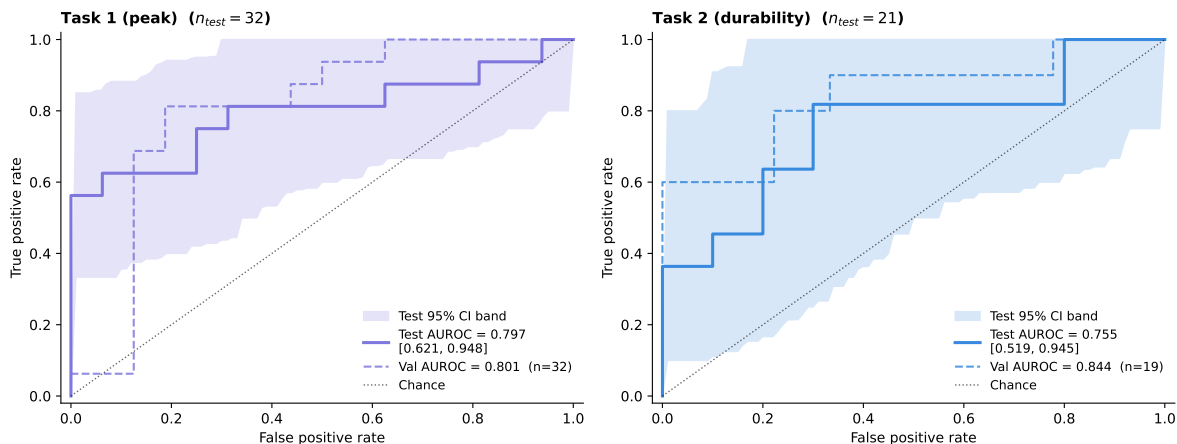


Fig 4. ROC curves on the held-out test set with 95% bootstrap confidence intervals, and validation-set ROCs for comparison. Left: Task 1 (peak response, $n_{\text{test}} = 32$); test AUROC 0.797 (95% CI [0.621, 0.948]), validation AUROC 0.801. **Right:** Task 2 (durability, $n_{\text{test}} = 21$); test AUROC 0.755 (95% CI [0.519, 0.945]), validation AUROC 0.844. Solid line: ROC on the observed test set. Shaded band: pointwise 95% confidence interval on the true positive rate at each false positive rate, from $B = 1000$ bootstrap resamples of the test set. Dashed line: validation-set ROC on the same trained model. Dotted diagonal: chance. Validation and test AUROC agree closely on Task 1 (0.801 vs 0.797). On Task 2 the validation AUROC (0.844) exceeds the test AUROC (0.755) by approximately 0.09. Given the small Task 2 test set ($n = 21$) and the use of validation AUROC for early stopping, this gap is consistent with mild optimism in validation-based model selection rather than a clear failure of generalization.

Predictive performance on both tasks

The preferred configuration achieves test AUROC 0.797 for Task 1 and 0.755 for Task 2 (Fig 4). Bootstrap 95% confidence intervals from 1000 resamples are [0.621, 0.948] for Task 1 and [0.519, 0.945] for Task 2; the full bootstrap distributions are shown in Fig 5. The Task 2 CI is comparably wide despite the smaller test set ($n = 21$ versus $n = 32$ for Task 1) because the durability signal is inherently noisier.

To verify these AUROCs reflect a genuine feature-label relationship rather than artifacts of the held-out split, we performed a joint label permutation test with $N = 1000$ retraining runs (Methods). The null distributions centered near chance (Task 1: mean 0.509, SD 0.098; Task 2: mean 0.501, SD 0.147), confirming the architecture does not produce above-chance performance in the absence of a learnable signal. The observed Task 1 AUROC of 0.797 exceeded all but a small fraction of null permutations ($p = 0.002$), sitting approximately 3.0 null-SDs above the null mean (Fig 6). The observed Task 2 AUROC of 0.755 exceeded the null at $p = 0.045$, approximately 1.7 null-SDs above the null mean. The wider Task 2 null distribution reflects the smaller labeled test subset; combined with the greater intrinsic difficulty of long-term retention prediction, this yields a less stringent significance result for Task 2 ($p = 0.045$) than for Task 1 ($p = 0.002$). Both results are significant at $\alpha = 0.05$, with Task 1 additionally significant at $\alpha = 0.01$.

Per-modality contribution: peak and durability rely on different signals

To diagnose what each modality contributes to the results, we conducted complementary leave-one-out (LOO) and keep-one-out (KOO) analyses on the trained model (Methods, Fig 7). Both analyses are evaluated on the complete-case subset of the test set (subjects with all four modalities measured), giving a reference test AUROC of 0.888 for Task 1 and 0.735 for Task 2; deviations from these references quantify modality contribution.

For Task 1 (peak response), the LOO and KOO analyses agree: *cytokine* is the dominant modality. It is the strongest single-modality predictor (KOO = 0.935, exceeding the all-modalities value of 0.888) and the

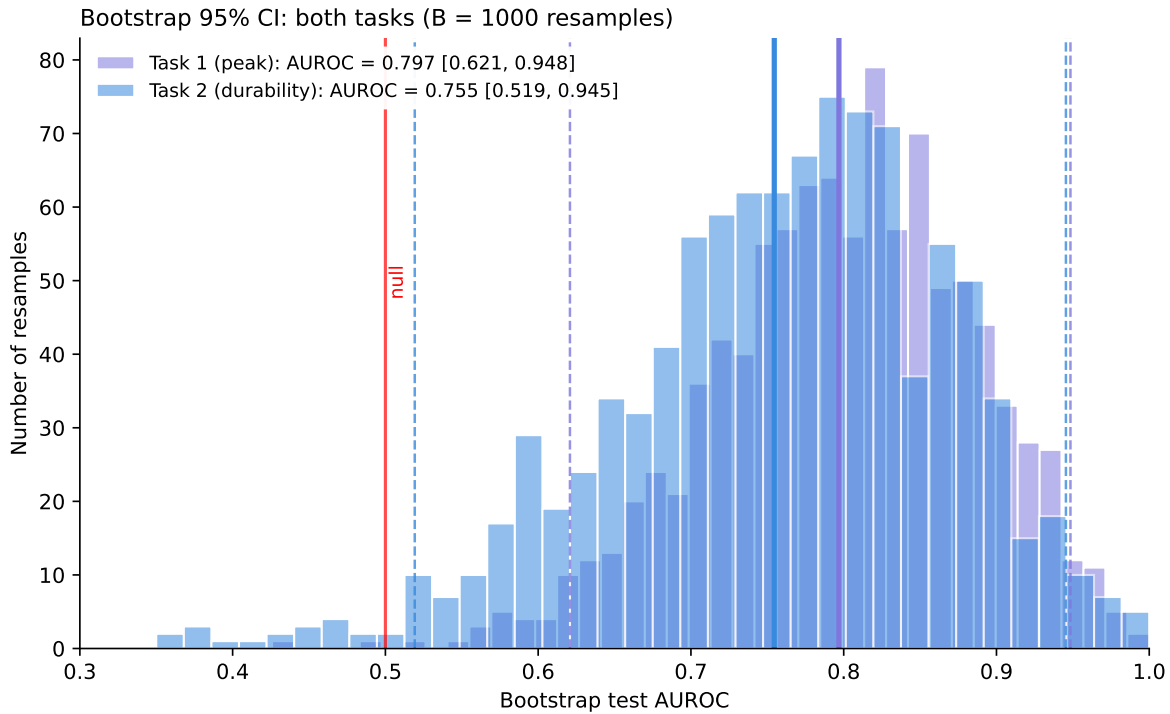


Fig 5. Bootstrap AUROC distributions on the held-out test set, both tasks overlaid. Histograms of test-set AUROC across $B = 1000$ bootstrap resamples (sampling subjects with replacement from the held-out test set, predictions held fixed). Task 1 (peak response, lavender): observed AUROC 0.797, 95% CI [0.621, 0.948]. Task 2 (durability, blue): observed AUROC 0.755, 95% CI [0.519, 0.945]. Solid coloured vertical lines: observed AUROC for each task. Dashed coloured vertical lines: 2.5th and 97.5th percentiles of the bootstrap distribution, defining the 95% percentile-method confidence interval. Red vertical line: null AUROC (0.5). The Task 2 distribution is wider than Task 1, reflecting the smaller test set ($n = 21$ vs $n = 32$).

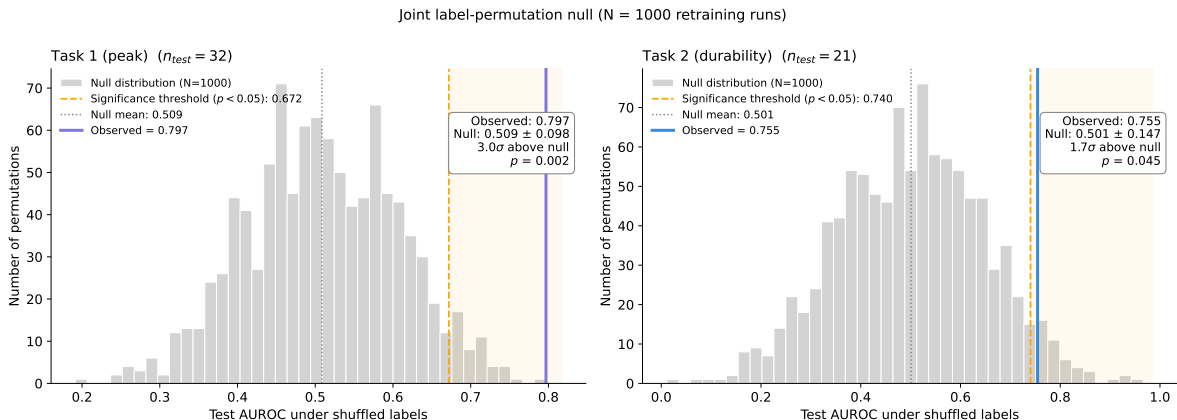


Fig 6. Label-permutation null distributions confirm learned signal for both tasks. Histograms of test-set AUROC across $N = 1000$ joint label permutations (both Task 1 and Task 2 labels shuffled; full pipeline retrained per permutation). The dashed orange line marks the significance threshold (95th percentile of the null, $p < 0.05$); the rejection region is shaded lightly. The dotted grey line marks the null mean. **Left:** Task 1 (peak response); observed AUROC 0.797 exceeds the null at $p = 0.002$, approximately 3.0 null-SDs above the null mean. **Right:** Task 2 (durability); observed AUROC 0.755 exceeds the null at $p = 0.045$, approximately 1.7 null-SDs above the null mean. Null means (Task 1: 0.509; Task 2: 0.501) sit near chance, confirming the permutation procedure is well-calibrated.

modality whose removal most harms the ensemble (LOO $\Delta = +0.068$). *Cell frequency* shows the opposite pattern: it is the weakest single-modality predictor (KOO = 0.783) and removing it from the ensemble *improves* test AUROC by 0.058 (LOO $\Delta = -0.058$), indicating that cell-frequency features add noise rather than signal at this sample size. Antibody and gene contribute modestly on both metrics (KOO 0.879 and 0.860; LOO +0.003 and +0.011).

For Task 2 (durability), the picture is qualitatively different. *Antibody* alone matches the full-ensemble performance (KOO = 0.735); cytokine, cell, and gene drop sharply in isolation (KOO 0.663, 0.664, 0.624). LOO drops are uniformly small (all within ± 0.02 of baseline), indicating that no single modality is strictly necessary, but antibody clearly carries the bulk of the durability signal.

This task-specific pattern emerges without any explicit supervision telling the model which modalities to weight for which task. The shared MLP and the joint contrastive loss together produce a representation in which different modality combinations are diagnostic for different downstream questions, consistent with the biology of peak response (driven by early innate cytokine signatures, which predict subsequent antibody outcomes across vaccines [12, 17]) versus durability (an antibody-centric long-term outcome sustained by long-lived plasma cells [1]).

Graceful degradation under inference-time missingness

Real-world deployment of multimodal models faces an unavoidable problem: new subjects may arrive with arbitrary subsets of modalities missing due to assay availability, sample quality, or cost. To probe how the trained model handles this situation, we simulated a range of inference-time modality-missingness rates ρ for each of the four modalities (Methods, Fig 8).

The trained model handles inference-time modality missingness with task-asymmetric tolerance. On Task 1, AUROC remains within ~ 0.02 – 0.03 of the all-modalities-present value across the full range of ρ for every modality, and all curves stay well above the meta-only baseline (0.58) even at $\rho = 1$; cell-frequency masking on Task 1 actually shows a slight upward trend rather than a decline (from 0.797 at $\rho = 0$ to 0.88 at $\rho = 1$). On Task 2 the safe-tolerance regime is narrower: AUROC stays close to (or slightly above) the all-modalities-present value as long as no more than $\sim 20\%$ of test subjects are missing any one modality. Beyond that, modalities separate sharply. Cytokine missingness is the most benign: it is in fact slightly beneficial in the $\rho \approx 0.2$ – 0.3 range, where the curve rises modestly above the all-modalities-present value

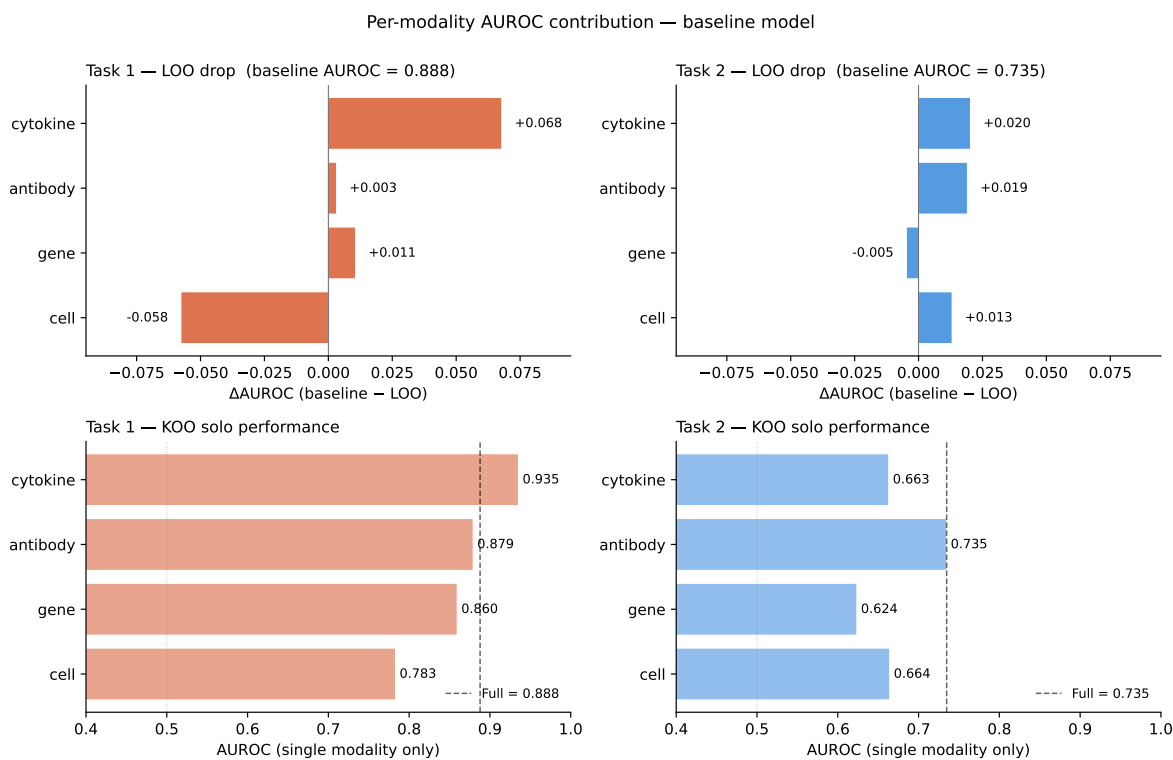


Fig 7. Per-modality contribution to peak and durability prediction. Top: Leave-one-out (LOO) analysis: change in test AUROC when each modality is masked out at inference, computed as $\Delta = \text{baseline AUROC} - \text{LOO AUROC}$. Positive values indicate the modality contributes to baseline performance; negative values indicate the modality is harmful to the ensemble. **Bottom:** Keep-one-out (KOO) analysis: test AUROC when only one modality is retained at inference. High values indicate standalone sufficiency. All-modalities AUROC is shown as a dashed reference line. For Task 1, cytokine dominates on both LOO (+0.068) and KOO (0.935), while cell frequency hurts the ensemble (LOO -0.058). For Task 2, antibody alone matches the full ensemble (KOO = 0.735). Both analyses are evaluated on the complete-case test subset.

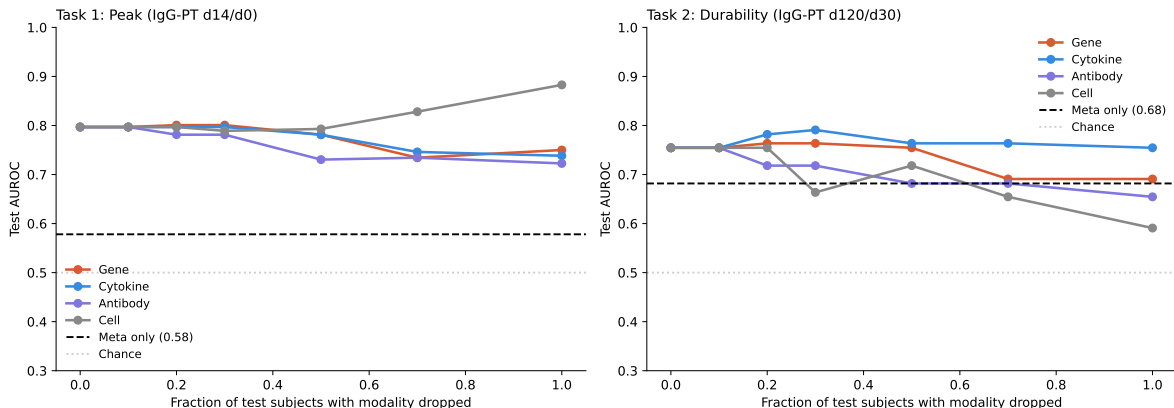


Fig 8. Graceful degradation under inference-time modality missingness. For each modality, a fraction ρ of test subjects have that modality randomly masked at inference, with attention renormalised over the remaining three. Test AUROC is computed at each $\rho \in \{0.0, 0.1, 0.2, 0.3, 0.5, 0.7, 1.0\}$ under a fixed masking seed (13). **Left:** Task 1 (peak response). **Right:** Task 2 (durability). Dashed black line: meta-only baseline (the model’s AUROC when all four modalities are masked, leaving only `infancy_vac` and biological sex). Dotted grey line: chance (0.5). On Task 1, all modality curves stay well above meta-only across the full range of ρ . On Task 2, only cytokine remains clearly above meta-only at $\rho = 1$; gene meets the meta-only line, while antibody and cell fall below it, with cell crossing meta-only by $\rho \approx 0.3$.

before settling back to ~ 0.755 at $\rho = 1$, consistent with cytokine carrying limited durability-specific signal in the ensemble (Fig 7). Gene reaches the meta-only baseline at $\rho = 1$ (~ 0.69). Antibody and cell drop below the meta-only baseline (0.66 and 0.59 respectively at $\rho = 1$); cell-frequency masking is the most damaging, ending clearly below meta-only at $\rho = 1$. In practical terms, a deployed model can be safely used on cohorts where any single modality is missing for up to $\sim 30\%$ of subjects on Task 1 or $\sim 20\%$ on Task 2; cell-frequency missingness in particular is the limiting deployment factor on durability prediction.

Architectural ablation

To quantify which architectural components matter, we trained four configurations of the model on the same fixed seed split: *Full (preferred)* with both contrastive loss and modality dropout active; *No contrastive* ($\lambda = 0$); *No modality dropout* ($p = 0$); and *Neither* (both removed). Test AUROC and 95% bootstrap CIs are shown in Table 3.

Both architectural components contribute substantively. Removing the contrastive loss drops Task 1 AUROC by 0.231 (from 0.797 to 0.566), the largest single-component effect. Removing modality dropout drops Task 1 AUROC by 0.176 (from 0.797 to 0.621). Notably, the configuration with neither component does not produce the worst result on Task 1: at 0.719, “Neither” is in fact *better* than either single-ablation configuration (“No contrastive” 0.566, “No modality dropout” 0.621). This non-monotone pattern indicates that contrastive loss and modality dropout interact: combining contrastive alignment with full-modality training (the “No modality dropout” case) yields a poorly conditioned representation that the contrastive loss further sharpens in an unhelpful direction; removing both components reverts to a less constrained but more robust configuration. The *Full* configuration, with both components active, is the only one that achieves AUROC above 0.79 on Task 1.

Task 2 results are flatter across configurations (range 0.609 to 0.755), with the *Full* configuration again the best. The relative robustness of Task 2 to ablation is consistent with its heavier reliance on the antibody modality alone (see Fig 7): when one component is removed, the antibody pathway through the shared MLP can still carry most of the durability signal.

A separate row in Table 3 probes the Task 2 loss weighting. At $w_{T2} = 1$ (no up-weighting), Task 1

AUROC drops to 0.668 and Task 2 to 0.673, declines of 0.129 and 0.082 respectively. The Task 1 effect is the larger one, which is the signature of multi-task transfer: properly weighting Task 2 during training yields a better-conditioned shared representation that benefits Task 1 prediction. This is direct evidence that multi-task co-training contributes to peak prediction at this sample size, complementing the contrastive-loss and modality-dropout ablations above.

Table 3. Architectural ablation: test-set AUROC with 95% bootstrap CIs. The full configuration includes both the dual-label contrastive loss ($\lambda = 0.1$) and modality dropout ($p = 0.4$), with Task 2 loss up-weighted at $w_{T2} = 2$. Each ablation row sets exactly one hyperparameter to its ‘off’ value ($\lambda = 0$, $p = 0$, or $w_{T2} = 1$) while keeping the others at preferred values. All variants use same fixed seed and the same hyperparameters otherwise.

Configuration	λ	p	w_{T2}	Task 1 AUROC [95% CI]	Task 2 AUROC [95% CI]
Full (preferred)	0.10	0.40	2.0	0.797 [0.621, 0.948]	0.755 [0.519, 0.945]
No contrastive	0.00	0.40	2.0	0.566 [0.344, 0.770]	0.682 [0.427, 0.900]
No modality dropout	0.10	0.00	2.0	0.621 [0.406, 0.824]	0.609 [0.346, 0.870]
Neither	0.00	0.00	2.0	0.719 [0.512, 0.910]	0.673 [0.398, 0.900]
No T2 up-weighting	0.10	0.40	1.0	0.668 [0.453, 0.863]	0.673 [0.423, 0.889]

Comparison to tabular baselines

To benchmark the multi-task fusion architecture, we trained three baseline classifiers (logistic regression, XGBoost, TabMLP) under two feature regimes: concatenated raw features with mean imputation, and concatenated TabPFN-v2 embeddings (Methods). The TabPFN-embedding baselines isolate the contribution of the architectural design from the contribution of the upstream feature extractor. Test-set AUROCs and bootstrap 95% confidence intervals are shown in Table 4.

On Task 1 (peak response), logistic regression on TabPFN embeddings achieves AUROC 0.816 ([0.659, 0.957]), narrowly exceeding the multi-task model’s 0.797 point estimate; the two CIs overlap heavily and the difference is not statistically distinguishable. TabMLP on TabPFN embeddings is also competitive at 0.785 ([0.623, 0.942]). This indicates that, for peak prediction alone, the per-modality TabPFN embeddings already carry most of the predictive signal, and several classifiers on their concatenation perform comparably to the full multi-task model. The remaining Task 1 baselines fall below ours: XGBoost on raw features (0.781), logistic regression and TabMLP on raw features (0.699 and 0.594, both with lower CI below chance), and XGBoost on TabPFN embeddings (degenerate at 0.500).

On Task 2 (durability), the picture is sharply different. The multi-task model achieves AUROC 0.755 ([0.519, 0.945]), substantially above all baselines on TabPFN embeddings: logistic regression drops to 0.609 ([0.336, 0.857], lower CI below chance), XGBoost to 0.364 (below chance), and TabMLP collapses to a degenerate constant predictor (0.500 across bootstrap resamples, indicating training failure at this sample size). The raw-feature baselines for Task 2 are stronger (logistic regression 0.791, TabMLP 0.777) but their Task 1 performance is correspondingly weak (0.699 and 0.594, both with lower CI below chance).

Read across both tasks, the multi-task fusion architecture is the only method whose 95% lower CI bound is above chance on both tasks simultaneously. Every baseline either (i) fails to clear chance on Task 1 (raw-feature logistic regression and TabMLP), (ii) fails to clear chance on Task 2 (raw-feature XGBoost; TabPFN-embedding logistic regression and XGBoost), or (iii) degenerates entirely on one of the two tasks (TabPFN-embedding XGBoost on Task 1, TabMLP on Task 2). At this sample size, with this feature complexity and label structure, joint above-chance reliability across both biologically dissociated tasks requires the architectural design choices made here.

Discussion

We addressed a challenging regime in precision vaccinology: predicting both peak and long-term phases of the humoral booster response from small, heterogeneous, partially missing multi-omic data. A multi-task

Table 4. Test-set AUROC: comparison to baselines on raw features and on TabPFN-v2 embeddings. Bootstrap 95% confidence intervals from 1000 resamples. Baselines are fit on training subjects ($n_{\text{train}} = 94$ for Task 1, $n_{\text{train}} = 56$ for Task 2) with default hyperparameters. The same seed for train/test split is used throughout. “Raw features” baselines use concatenated raw features from all four modalities with per-feature training-set mean imputation; “TabPFN emb.” baselines use concatenated 1,536-dimensional TabPFN-v2 embeddings (one per modality, total 6,144 dimensions). Bold: best point estimate per task; †: lower 95% CI bound below 0.5; ‡: degenerate predictor (constant output, AUROC fixed at 0.5 across all bootstrap resamples).

Method	Task 1 AUROC [95% CI]	Task 2 AUROC [95% CI]
<i>Raw features (mean-imputed concatenation)</i>		
Logistic regression	0.699 [0.495, 0.867] [†]	0.791 [0.555, 0.959]
XGBoost	0.781 [0.599, 0.929]	0.645 [0.382, 0.870] [†]
TabMLP	0.594 [0.384, 0.801] [†]	0.777 [0.526, 1.000]
<i>TabPFN-v2 embeddings (concatenation)</i>		
Logistic regression	0.816 [0.659, 0.957]	0.609 [0.336, 0.857] [†]
XGBoost	0.500 [0.500, 0.500] [‡]	0.364 [0.214, 0.500] ^{†,‡}
TabMLP	0.785 [0.623, 0.942]	0.500 [0.500, 0.500] [‡]
Preferred (ours)	0.797 [0.621, 0.948]	0.755 [0.519, 0.945]

contrastive fusion architecture recovered predictive signal for both phases (test AUROC 0.797 for peak, 0.755 for durability), with both AUROCs significantly above chance under joint label permutation ($p = 0.002$ and $p = 0.045$ over $N = 1000$ permutations).

The two clinical endpoints are anti-correlated (Spearman $r = -0.580$, Cohen’s $\kappa = -0.520$), with most subjects sorting into two response groups: large but fading, or modest but better retained. The low peak / low durability quadrant is essentially empty ($n = 4$), indicating that immune systems rarely fail on both axes simultaneously. This dissociation is consistent with the canonical two compartment biology of acute versus long-term humoral responses [1,2] and is what motivates a multi-task framing rather than single-task prediction of either phase alone.

Per-modality contribution analyses reveal that the trained model routes the two tasks to different modalities. For peak prediction, cytokine dominates: standalone AUROC 0.935 exceeds the all-modalities value (0.888), and removing cytokine causes the largest LOO drop (0.068). Cell frequency is the weakest standalone predictor (0.783) and its removal slightly *improves* ensemble performance, suggesting cell-frequency features are either redundant with cytokine or actively noisy at this sample size. For durability prediction, antibody alone matches the full-ensemble value (0.735) while cytokine and cell drop sharply in isolation (0.663, 0.664). This task-specific routing is biologically coherent: peak response at day 14 reflects acute B-cell activation and plasmablast expansion, for which plasma cytokine signatures are direct mechanistic markers [12,17], whereas durability at day 120 depends on long-lived plasma cell maintenance, a process most directly captured by the antibody titer trajectory itself [1]. The model recovers this underlying signature without supervision on which modalities should matter for which task.

The architectural ablation directly tests whether multi-task co-training contributes to peak prediction. At $w_{T2} = 2$ (preferred), Task 1 AUROC is 0.797; at $w_{T2} = 1$, it drops to 0.668, a decline of 0.129. This is direct evidence that the Task 2 head acts as a regulariser on the shared backbone: forcing the representation to also support durability prediction prevents over-fitting to peak-specific idiosyncrasies, despite the two tasks being biologically anti-correlated. The contrastive loss and modality dropout components contribute on top of this base multi-task benefit (Table 3); all three are necessary to recover above-0.79 Task 1 AUROC.

The TabPFN-embedding baseline comparison clarifies the architectural design’s distinctive contribution. On Task 1, the multi-task model and the strongest TabPFN-embedding baselines achieve comparable AUROC (logistic regression 0.816, TabMLP 0.785, multi-task 0.797), with overlapping CIs. This is consistent with the contribution analysis: peak is dominated by a single highly informative modality that a linear classifier on TabPFN embeddings can exploit directly. On Task 2, every baseline either falls below chance or degenerates: durability requires integration across modalities and a label structure (the dual-label supervised contrastive loss) that no concatenation baseline can access. The multi-task architecture is therefore the only

method tested that delivers above-chance performance on both tasks simultaneously, and this joint reliability is its distinctive contribution. The raw-feature baselines also face a structural disadvantage in handling missingness: with up to 38.6% of subjects missing certain modalities, mean imputation fills entire modality blocks with training-set averages, producing biased input vectors for those subjects. The attention-based fusion in our architecture sidesteps this by excluding absent modalities from the softmax computation rather than imputing them.

The framework is naturally extensible to external validation cohorts and to other vaccines for which similar multi-omic profiling exists, allowing future tests of whether the peak-durability dissociation and task-specific modality patterns reported here generalize beyond CMI-PB and beyond pertussis.

Limitations

This study has the following limitations. First, the sample size is small ($n = 158$ subjects with a Task 1 label, $n = 96$ in the modeled Task 2 subset; $n_{\text{test}} = 32$ and $n = 21$ in the held-out test sets respectively), reflecting the reality of longitudinal multi-omic human vaccine studies but producing wide bootstrap confidence intervals on test AUROC, especially for Task 2. We address this with permutation testing to confirm both AUROCs are above chance, but a larger validation cohort will be needed before clinical interpretation. Second, cross-cohort transportability has not been directly assessed: training on 2020-2022 and testing on 2023 would be a natural test, but is constrained by the absence of Task 2 labels in the 2023 cohort. External validation on independent multi-omic vaccine cohorts remains a goal for future work. Third, the per-modality contribution analyses (LOO and KOO) describe the behavior of a single trained model and should be interpreted as descriptions of *this* model’s contributions rather than universal biological claims; finer-grained, feature-level attribution within each modality is deferred to future work.

Data and code availability

The CMI-PB data used in this study are publicly available through the CMI-PB resource [3] at <https://www.cmi-pb.org>. Code to reproduce the analyses is available at <https://github.com/Divya1205/cmi-pb-multitask>.

Acknowledgments

I thank the CMI-PB consortium for generating, harmonizing, and openly sharing the longitudinal multi-omic pertussis booster vaccination dataset that made this work possible, and Dr. Pramod Shinde for helpful discussions and guidance on the dataset.

References

1. Amanna IJ, Carlson NE, Slifka MK. Duration of humoral immunity to common viral and vaccine antigens. *New England Journal of Medicine*. 2007;357(19):1903–1915.
2. Gillard J, Suffiotti M, Brazda P, Venkatasubramanian PB, Versteegen P, de Jonge MI, et al. Antiviral responses induced by Tdap-IPV vaccination are associated with persistent humoral immunity to *Bordetella pertussis*. *Nature Communications*. 2024;15(1):2133.
3. Shinde P, Soldevila F, Reyna J, Aoki M, Rasmussen M, Willemsen L, et al. A multi-omics systems vaccinology resource to develop and test computational models of immunity. *Cell Reports Methods*. 2024;4(3):100731.
4. Mooi FR, Van Der Maas NAT, De Melker HE. Pertussis resurgence: waning immunity and pathogen adaptation: two sides of the same coin. *Epidemiology & Infection*. 2014;142(4):685–694.

5. Domenech de Cellès M, Rohani P. Pertussis vaccines, epidemiology and evolution. *Nature Reviews Microbiology*. 2024;22(11):722–735.
6. Warfel JM, Zimmerman LI, Merkel TJ. Acellular pertussis vaccines protect against disease but fail to prevent infection and transmission in a nonhuman primate model. *Proceedings of the National Academy of Sciences*. 2014;111(2):787–792.
7. Sheridan SL, Frith K, Snelling TL, Grimwood K, McIntyre PB, Lambert SB. Waning vaccine immunity in teenagers primed with whole cell and acellular pertussis vaccine: recent epidemiology. *Expert Review of Vaccines*. 2014;13(9):1081–1106.
8. McCarthy KN, Hone S, McLoughlin RM, Mills KHG. IL-17 and IFN- γ -producing respiratory tissue-resident memory CD4 T cells persist for decades in adults immunized as children with whole-cell pertussis vaccines. *The Journal of Infectious Diseases*. 2024;230(3):e518–e523.
9. da Silva Antunes R, Babor M, Carpenter C, Khalil N, Cortese M, Mentzer AJ, et al. Th1/Th17 polarization persists following whole-cell pertussis vaccination despite repeated acellular boosters. *Journal of Clinical Investigation*. 2018;128(9):3853–3865.
10. Wilk MM, Borkner L, Misiak A, Curham L, Allen AC, Mills KHG. Immunization with Whole Cell but Not Acellular Pertussis Vaccines Primes CD4 T_{RM} Cells That Sustain Protective Immunity Against Nasal Colonization with *Bordetella pertussis*. *Emerging Microbes & Infections*. 2019;8(1):169–185.
11. da Silva Antunes R, Soldevila F, Pomaznoy M, Babor M, Bennett J, Tian Y, et al. A system-view of *Bordetella pertussis* booster vaccine responses in adults primed with whole-cell versus acellular vaccine in infancy. *JCI Insight*. 2021;6(7):e141023.
12. Querec TD, Akondy RS, Lee EK, Cao W, Nakaya HI, Teuwen D, et al. Systems biology approach predicts immunogenicity of the yellow fever vaccine in humans. *Nature Immunology*. 2009;10(1):116–125.
13. Hollmann N, Müller S, Eggensperger K, Hutter F. TabPFN: A Transformer That Solves Small Tabular Classification Problems in a Second. *arXiv preprint arXiv:220701848*. 2022;.
14. Hollmann N, Müller S, Purucker L, Krishnakumar A, Körfer M, Hoo SB, et al. Accurate predictions on small data with a tabular foundation model. *Nature*. 2025;637(8045):319–326.
15. Troyanskaya O, Cantor M, Sherlock G, Brown P, Hastie T, Tibshirani R, et al. Missing value estimation methods for DNA microarrays. *Bioinformatics*. 2001;17(6):520–525.
16. Johnson WE, Li C, Rabinovic A. Adjusting batch effects in microarray expression data using empirical Bayes methods. *Biostatistics*. 2007;8(1):118–127.
17. Pulendran B. Systems Vaccinology: Probing Humanity’s Diverse Immune Systems with Vaccines. *Proceedings of the National Academy of Sciences*. 2014;111(34):12300–12306.
18. Nakaya HI, Wrammert J, Lee EK, Racioppi L, Marie-Kunze S, Haining WN, et al. Systems Biology of Vaccination for Seasonal Influenza in Humans. *Nature Immunology*. 2011;12(8):786–795.
19. Li S, Roupheal N, Duraisingham S, Romero-Steiner S, Presnell S, Davis C, et al. Molecular Signatures of Antibody Responses Derived from a Systems Biology Study of Five Human Vaccines. *Nature Immunology*. 2014;15(2):195–204.
20. Edwards KM, Decker MD. Pertussis Vaccines. In: Plotkin SA, Orenstein WA, Offit PA, Edwards KM, editors. *Plotkin’s Vaccines*. 7th ed. Philadelphia: Elsevier; 2018. .
21. Burdin N, Handy LK, Plotkin SA. What Is Wrong with Pertussis Vaccine Immunity? The Problem of Waning Effectiveness of Pertussis Vaccines. *Cold Spring Harbor Perspectives in Biology*. 2017;9(12):a029454.

22. Khosla P, Teterwak P, Wang C, Sarna A, Tian Y, Isola P, et al. Supervised Contrastive Learning. In: Advances in Neural Information Processing Systems (NeurIPS). vol. 33; 2020. p. 18661–18673.
23. Loshchilov I, Hutter F. Decoupled Weight Decay Regularization. In: International Conference on Learning Representations (ICLR); 2019. .
24. Ojala M, Garriga GC. Permutation Tests for Studying Classifier Performance. Journal of Machine Learning Research. 2010;11:1833–1863. Available from: <https://jmlr.org/papers/v11/ojala10a.html>.
25. Pedregosa F, Varoquaux G, Gramfort A, Michel V, Thirion B, Grisel O, et al. Scikit-learn: Machine Learning in Python. Journal of Machine Learning Research. 2011;12:2825–2830.
26. Chen T, Guestrin C. XGBoost: A Scalable Tree Boosting System. In: Proceedings of the 22nd ACM SIGKDD International Conference on Knowledge Discovery and Data Mining. KDD '16. ACM; 2016. p. 785–794.